A Unified Framework for Delineation of Ambulatory Holter ECG Events via Analysis of a Multiple-Order Derivative Wavelet-Based Measure

M. R. Homaeinezhad*, A. Ghaffari*, H. Najjaran Toosi*, M. Tahmasebi** and M. M. Daevaeiha***

Abstract: In this study, a new long-duration holter electrocardiogram (ECG) major events detection-delineation algorithm is described operating based on the false-alarm error bounded segmentation of a decision statistic with simple mathematical origin. To meet this end, first three-lead holter data is pre-processed by implementation of an appropriate bandpass finite-duration impulse response (FIR) filter and also by calculation of the Euclidean norm between corresponding samples of three leads. Then, á trous discrete wavelet transform (DWT) is applied to the resulted norm and an unscented synthetic measure is calculated between some obtained dyadic scales to magnify the effects of low-power waves such as P or T-waves during occurrence of arrhythmia(s). Afterwards, a uniform length window is slid sample to sample on the synthetic scale and in each slid, six features namely as summation of the nonlinearly amplified Hilbert transform, summation of absolute first order differentiation, summation of absolute second order differentiation, curve length, area and variance of the excerpted segment are calculated. Then all feature trends are normalized and superimposed to yield the newly defined multiple-order derivative wavelet based measure (MDWM) for the detection and delineation of ECG events. In the next step, a α-level Neyman-Pearson classifier (which is a false-alarm probability-FAP controlled tester) is implemented to detect and delineate QRS complexes. To show advantages of the presented method, it is applied to MIT-BIH Arrhythmia Database, QT Database, and T-Wave Alternans Database and as a result, the average values of sensitivity and positive predictivity Se = 99.96% and P+ = 99.96% are obtained for the detection of QRS complexes, with the average maximum delineation error of 5.7 msec, 3.8 msec and 6.1 msec for P-wave, QRS complex and T-wave, respectively showing marginal improvement of detection-delineation performance. In the next step, the proposed method is applied to DAY hospital high resolution holter data (more than 1,500,000 beats including Bundle Branch Blocks-BBB, Premature Ventricular Complex-PVC and Premature Atrial Complex-PAC) and average values of Se=99.98% and P+=99.97% are obtained for QRS detection. In summary, marginal performance improvement of ECG events detection-delineation process in a widespread values of signal to noise ratio (SNR), reliable robustness against strong noise, artifacts and probable severe arrhythmia(s) of high resolution holter data and the processing speed 163,000 samples/sec can be mentioned as important merits and capabilities of the proposed algorithm.

Keywords: ECG Detection-Delineation, First-Order Derivative, Second-Order Derivative; Discrete Wavelet Transform; Multi Lead Analysis, Hilbert transform, Curve Length; Variance, Neyman-Pearson Hypothesis Test; False Alarm Probability.

1 Introduction

Heart is a special muscle which its constitutive cells (myocytes) possess two important characteristics namely as nervous excitability and mechanical tension with force feedback. The superposition of all myocytes electrical activity on the skin surface results a detectable potential difference which its detection and registration is called electrocardiography [1]. If according to any happening, nervous and/or mechanical function of a region of myocytes encounter with failure, the corresponding abnormal effects will appear in the ECG signal and in the heart hemodynamic performance. Today, 24 (48) hour ECG holters with high sampling frequency are widely used in ICUs to monitor and assess patients heart long-term function(s). Although, holter monitoring has remarkable merits, in high sampling rates, for a short or long time duration, strong noise and motion artifacts may be seen in some channels of holter data which decrease performance accuracy of implemented ECG events detector. On the other hand, statistical analysis of ECG parameters in long-term conditions can yield acceptable solutions for diagnosis of some certain phenomena such as T-Wave Alternans (TWA) [2,3], Atrial Fibrillation (AF) [4,5], QT-prolongation [6]. In addition, proper delineation of ECG waveforms can help to achieve more accurate results in applications such as pattern recognition or arrhythmia clustering and classification [7,8]. Therefore, parameterization and detection of ECG signal events using a reliable algorithm is the first stage in the computer analysis of the ECG signal. Numerous approaches have yet been developed for the aim of detection of the ECG events including mathematical models [9], Hilbert transform and the first derivative [10,11], second order derivative [14], wavelet transform and the filter banks [15-17], soft computing (Neuro-fuzzy, genetic algorithm) [18], Hidden Markov Models (HMM) application [19], etc. The performance of QRS detection algorithms can easily be verified using the standard databases such as MIT-BIH Arrhythmia Database [20]; however, validation of a proposed algorithms for the detection-delineation of P and T-waves has turned to a difficult problem due to the lack of a gold standard as universal reference [15]. The wavelet transform has three appropriate and useful properties; first, using this approach the original signal can be described in different time scales and therefore different spatial resolutions would be achieved. For instance, in the scale 2^1, the high energy waves (such as QRS complex) can be easily distinguished from other waves; however, in the scale 2^4 or 2^5, weak or very weak waves (such as T-wave P-wave or probable U-waves) can be detected [16]. Thus, using a multi-step algorithm it would be possible to detect strong, weak and very weak waves. This feature should be noted as one of the most significant characteristics of the wavelet transform which can be implemented to obtain more accurate results. Second, factors such as noise, artifacts, and baseline wandering can be distinguished from heart electrical activity based on their specific frequency contents which lead to better performance for the detection algorithm. Third, the wavelet transform can be easily implemented in practical cases due to the fact that it is a cascade consisting of sequential short length unit impulse response digital Finite-duration Impulse Response (FIR) filters. The algorithms already developed in this area, such as [15-17], achieve acceptable results in the area of QRS detection, Finding the location of J and fiducial points, the beginning of P-wave as well as the peak and end of T-wave. Applying some modifications to these methods, more innovative and more accurate approaches can be developed in the area of wave detection and delineation. By adding some innovations and modifications to previous methods, it would be possible to apply them to more challenging data including ambulatory holter ECG data which contains high-level noise and strong motion artifacts as well as severe arrhythmia with abnormal morphologies such as PVCs, PACs, a combination of these two, multifocal PVCs with complicated morphologies, etc. The corrections considered to be added to the previous methods, will make them more safe and robust in these cases, [16].

The results of the proposed detection algorithm were finally compared with the clinical manual annotations of different databases such as MIT-BIH Arrhythmia Database (F_s=360Hz) [20], QT (F_s=250Hz) [21], and TWA Challenge 2008 Database (F_s=500Hz) [23] as well as high resolution Holter data (MEDSET®-1000Hz, 3-Channel, 32-bits) [16-17]. As a result, the average values of sensitivity and positive predictivity Se = 99.96% and P+ = 99.96% are obtained for the detection of QRS complexes, with the average maximum delineation error of 5.7 msec, 3.8 msec and 6.1 msec for P-wave, QRS complex and T-wave, respectively. In the next step, the proposed method is applied to DAY hospital high resolution holter data (including BBB, PVC and PAC) and average values of Se=99.98% and P+=99.97% are obtained for sensitivity and positive predictivity respectively. The organization of paper is arranged as follow. In section 2, DWT pre-processing via à trous method and the MDWM structure with corresponding elements are described. In section 3, technical information of the implemented databases, obtained results from application of detection-delineation algorithm, and procedure of verification of the MDWM -based detection-delineation method are extensively illustrated. Finally, in section 4, some conclusions obtained during fulfillment of this study will be presented.

List of Abbreviations is as follows:

RCA:	Retrograde Conduction into Atrium
FCP:	Full Compensatory Pause
BBB:	Bundle Branch Block
TP:	True Positive
P+:	Positive Predictivity (%)

Se: Sensitivity (%)
SMF: Smoothing Function
FIR: Finite-duration Impulse Response
LE: Location Error
MDWM: Multiple-order Derivative Wavelet based Measure
HT: Hilbert Transform
FAP: False Alarm Probability
pdf: Probability Density Function
LR: Likelihood Ratio
ECG: Electrocardiogram
DWT: Discrete Wavelet Transform
SNR: Signal to Noise Ratio
QTDB: QT Database
MITDB: MIT-BIH Arrhythmia Database
TWADB: T-wave alternans Database
FP: False Positive
FN: False Negative
PVC: Premature Ventricular Contraction
PAC: Premature Atrial Contraction
CHECK#0: Procedure of evaluating obtained results using MIT-BIH annotation files
CHECK#1: Procedure of evaluating obtained results consulting with a control cardiologist
CHECK#2: Procedure of evaluating obtained results consulting with a control cardiologist and also at least with 3 residents

2 Materials and Methods

2.1 Discrete Wavelet Transform Using à Trous Method

Generally, it can be stated that the wavelet transform is a quasi-convolution of the hypothetical signal $x(t)$ and the wavelet function $\psi(t)$ with the dilation parameter a and translation parameter b, as follows

$$W_{a^x}(b) = \frac{1}{\sqrt{a}} \int_{-\infty}^{+\infty} x(t)\,\psi\big((t-b)/a\big)dt, \ a > 0 \tag{1}$$

The parameter a can be used to adjust the wideness of the basis function and therefore the transform can be adjusted in temporal resolutions. Suppose that the function $Y_{a^x}(b)$ is obtained based on a quasi-convolution of signal $x(t)$ and function $\theta(t)$, as follows

$$Y_{a^x}(b) = \int_{-\infty}^{+\infty} x(t)\,\theta\big((t-b)/a\big)dt \tag{2}$$

If the derivative of $Y_{a^x}(b)$ is calculated relative to b, then

$$\frac{\partial Y_{a^x}(b)}{\partial b} = -\frac{1}{a}\int_{-\infty}^{+\infty} x(t)\,\theta'\big((t-b)/a\big)dt \tag{3}$$

On the other hand, if $\psi(t)$ is the derivative of a smoothing function $\theta(t)$, i.e. $\psi(t) = \theta'(t)$, then

$$W_{a^x}(b) = -\frac{1}{\sqrt{a}}\frac{\partial Y_{a^x}(b)}{\partial b} \tag{4}$$

Accordingly, it can be concluded that wavelet transform at the scale a is proportional to the quasi-convolution derivative of the signal $x(t)$ and the smoothing function $\theta(t)$. Therefore, if wavelet transform of the signal crosses of zero, it will be an indicative of local extremum(s) existence in the smoothed signal and the absolute maximum value of the wavelet transform in different scales represents a maximum slope in the filtered signal. Thus, useful information can be obtained using wavelet transform in different scales. If the scale factor a and the translation parameter b are considered as $a = 2^k$ and $b = 2^k l$, the dyadic wavelet with the following basis function will be resulted [15],

$$\psi_{k,l}(t) = 2^{-k/2}\psi(2^{-k}t - l); \ k, l \in Z^+ \tag{5}$$

To implement the à trous wavelet transform algorithm, filters $H(z)$ and $G(z)$ should be used according to the block diagram represented in Fig. 1, [15]. According to this block diagram, each smoothing function (SMF) is obtained by sequential low-pass filtering (convolving with $H(z^{2k})$ filters), while after high-pass filtering of a SMF (convolving with $G(z^{2k})$ filters), the corresponding DWT at appropriate scale is generated.

For a prototype wavelet $\psi(t)$ with the following quadratic spline Fourier transform,

$$\Psi(\Omega) = j\Omega \left(\frac{\sin(\Omega/4)}{\Omega/4}\right)^4 \tag{6}$$

the transfer functions $H(z)$ and $G(z)$ can be obtained from the following equation

$$H(e^{j\omega}) = e^{j\omega/2}\left(\cos(\omega/2)\right)^3$$
$$G(e^{j\omega}) = 4je^{j\omega/2}\left(\sin(\omega/2)\right) \tag{7}$$

and therefore,

$$h[n] = (1/8)\{\delta[n+2] + 3\delta[n+1] + 3\delta[n] + \delta[n-1]\}$$
$$g[n] = 2\{\delta[n+1] - \delta[n]\} \tag{8}$$

It should be noted that for frequency contents of up to 50 Hz, the à trous algorithm can be used in different sampling frequencies. Therefore, one of the most prominent advantages of the à trous algorithm is the approximate independency of its results from sampling frequency. This is because of the main frequency contents of the ECG signal concentrate on the range less than 20 Hz [15,16]. After examination of various databases with different sampling frequencies (range between 136 to 10 kHz), it has been concluded that in low sampling frequencies (less than 750 Hz), scales 2^λ ($\lambda=1,2,\ldots,5$) are usable while for sampling frequencies more than 750 Hz, scales 2^λ ($\lambda=1,2,\ldots,8$) contain profitable information that can be used for the purpose of wave detection, delineation and classification.
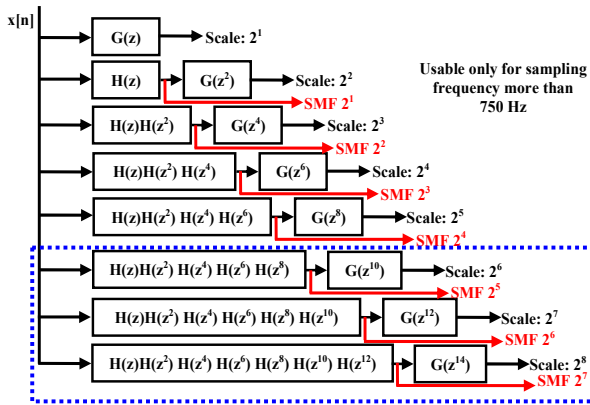
Fig. 1 FIR filter-bank implementation to generate discrete wavelet dyadic scales and smoothing functions transform based on à trous algorithm.

2.2 The Structure of Multiple-Order Derivative Wavelet-Based Measure (MDWM)

Nonlinearly amplified Hilbert transform (HT), first and second order derivatives, curve length, area and second order statistical moment (variance) are the basic constitutive elements of the MDWM. Below, some justifications for the selection of each measure are presented.

2.2.1 Summation of Nonlinearly Amplified Hilbert Transform

A quadrature filter with the following transfer function is called Hilbert transform (HT) which is an all-pass filter that changes the phase of the input signal -90^0 and has an impulse response of $1/(\pi t)$ [15],

$$G(\omega) = -j \, \text{sign}(\omega) = \begin{cases} -j & \omega > 0 \\ 0 & \omega = 0 \\ +j & \omega < 0 \end{cases} \qquad (9)$$

Therefore, the Hilbert transform of the signal $s(t)$ can be obtained from the following convolution,

$$s_H(t) = s(t) * \frac{1}{\pi t} = \frac{1}{\pi} \int_{-\infty}^{+\infty} \frac{s(\lambda)}{t-\lambda} d\lambda \qquad (10)$$

The most significant characteristic of Hilbert transform is its mapping of local maxima and minima values of the original signal to the values crossing of the zero, [15, 16].

As previously abovementioned, the HT rotates -90° the phase of its input signal, therefore, if the hypothetical signal $x(t)$ is represented by the Fourier series expansion $\hat{x}(t)$ [33], as follows

$$x(t) \approx \hat{x}(t) = \sum_{n=0}^{+\infty} X_n \sin(\omega_n t + \phi_n) \qquad (11)$$

where X_n and ϕ_n are the n-th term of the Fourier series expansion amplitude and phase, respectively. The approximate HT $\hat{x}_H(t)$ of the original signal $x(t)$ can be obtained as follows

$$x_H(t) \approx \hat{x}_H(t) = H[\hat{x}(t)] = H\left[\sum_{n=0}^{+\infty} X_n \sin(\omega_n t + \phi_n)\right]$$
$$= \sum_{n=0}^{+\infty} X_n \sin(\omega_n t + \phi_n - \pi/2) = -\sum_{n=0}^{+\infty} X_n \cos(\omega_n t + \phi_n) \qquad (12)$$

According to Eq. 12, it is seen that if signal $x(t)$ crosses from its absolute extremum points, then by rotation of the argument phase $\omega_n t + \phi_n$ by -90°, then the dominant value of the trigonomic components will push the $x_H(t)$ signal to cross from zero [11-12]. For instance, in Fig. 2, a generic test signal $x(t) = \sum_{n=1}^{2} X_n \sin(\omega_n t + \phi_n)$ given $X_1 = 1.0$, $X_2 = 1.25$, $\omega_1 = 7.85$, $\omega_2 = 4.712$, $\phi_1 = 0$, $\phi_2 = 7.2°$, and its HT is shown to numerically validate the aforementioned property of the HT. In the next step, by application a nonlinear exponential transformation to the HT of the original signal $x(t)$ as follows, the zero crossing locations of the HT are amplified while other points are pushed toward zero

$$x_N(t) = \exp\left(-\xi \, |x_H(t)|\right), \quad \xi > 0 \qquad (13)$$

where ξ is attenuation coefficient and if chosen large enough, only zero crossing (or zero vicinity) locations of the $x_H(t)$ are magnified toward unity while other points are pushed to zero. In other words, if $x(t)$ curve includes absolute extremums, the $x_H(t)$ will approximately be greater than zero in the vicinity of each absolute extremum location. According to this conclusion, in the k-th slid of the analysis window with the length of W_L samples, the HT based measure can be obtained from following summation

$$M_H(k) = \sum_{t=k}^{k+W_L} x_N(t) \qquad (14)$$

From another point of view, $M_H(k)$ shows the number of impulses occurred in the analysis window.

2.2.2 Summation of Absolute First-Order Derivative

If signal $x(t)$ is sampled from the continuous waveform by sampling frequency F_s, then the summation of absolute first order derivative of $x(t)$ signal in the analysis window is obtained as

$$M_{dff}(k) = F_s \sum_{t=k}^{k+W_L-1} \left[|x(t+1) - x(t)| \right] \qquad (15)$$

This measure clearly detects the activity extent of the high-frequency components of the original signal. In other words, in weak P or T-waves, in which their amplitude and area are not large enough, this quantity shows better sensitivity to such phenomena.

2.2.3 Summation of the Absolute Second-Order Derivative

Summation of the absolute second-order derivative of the signal $x(t)$ with the sampling frequency F_s, in the k-th slid of the analysis window can be obtained as

$$M_{dfII}(k) = F_s^2 \sum_{t=k}^{k+W_L-2} \left[\left| x(t+2) - 2x(t+1) + x(t) \right| \right] \qquad (16)$$

This measure indicates the ascend/descend rate or kurtosis of the signal $x(t)$ and detects the activity period of the source generating signal. The measure $M_{dfII}(k)$ shows remarkable fluctuations during activity of the heart individual events. A large value of M_{dfI} and M_{dfII} indicates a sharp transition from low to high or from high to low value in the excerpted segment. Consequently, these measures detect the probable edges of the signal in the analysis window. So, this quantity makes the MDWM sensitive to behavior of the signal in the edges.

2.2.4 Curve Length (Nonlinear First-Order Derivative)

Curve length of the signal $x(t)$ in the k-th slid of the analysis window is obtained approximately as [16, 17]

$$M_{CL}(k) \approx \frac{1}{F_s} \sum_{t=k}^{k+W_L-1} \sqrt{1 + \left[\left(x(t+1) - x(t) \right) F_s \right]^2} \qquad (17)$$

The curve length is suitable to measure the duration of the signal $x(t)$ events, either being strong or weak.

2.2.5 Area under Curve

The approximate area under curve $x(t)$ in the k-th slid of the analysis window is obtained from the following equation

$$M_{AR}(k) \approx \frac{1}{F_s} \sum_{t=k}^{k+W_L} \left| x(t) \right| \qquad (18)$$

2.2.6 Centralized Mean Square Value

An estimate of the centralized mean square value of the excerpted segment of signal $x(t)$ can be obtained as
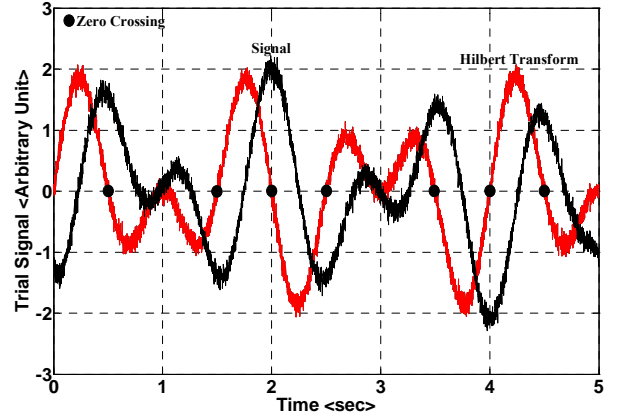
$$M_{MS}(k) = \frac{1}{W_L} \sum_{t=k}^{k+W_L} \left[x(t) - \mu_k \right]^2 \qquad (19)$$

where μ_k is the sample mean of the $x(t)$ in the analysis window that can be obtained from the following equation

$$\mu_k = \frac{1}{W_L} \sum_{t=k}^{k+W_L} x(t) \qquad (20)$$

The physical meaning of the $M_{MS}(k)$ is the average power of the events while this quantity graphically shows the dispersion of the samples around the mean value [13]. The $M_{MS}(k)$ indicates difference between

Fig. 2 Illustration of the main characteristic property of the HT of an embedded in noise signal. This figure shows that by crossing of the original signal from its extremums, equivalently the HT of the signal crosses from zero value.

absolute maximum and minimum values of an excerpted segment. This difference may not be seen via mean value because it is possible that the mean of a segment is a small value whilst the difference between its maximum and minimum values is large.

2.2.7 Construction of the multiple-order derivative wavelet based measure (MDWM)

The MDWM is the superposition of all calculated measures effect. However it should be noted that the largeness extent (order) of the $M_j(k)$, $j = H$, dfI, dfII, CL, AR, MS are not analogous to each other and sometimes one may be greater more than 1000 times from other(s), therefore, by superposing all raw trends, the effect of relatively small quantities are vanished from the MDWM. To solve this problem, if $\mathbf{M}_j$, $j = H$, dfI, dfII, CL, AR, MS the vector consisting of the $M_j(k)$ components with sample standard deviation σ_j, it can be shown that the new measures $\mathbf{M}_j^N = \mathbf{M}_j / \sigma_j$ $j = H$, dfI, dfII, CL, AR, MS are of unity variance, i.e.,

$$E[\mathbf{M}_j / \sigma_j] = \mu_j / \sigma_j \Rightarrow E[\underbrace{(\mathbf{M}_j / \sigma_j - \mu_j / \sigma_j)^2}_{\mathbf{M}_j^N}] \qquad (21)$$

$$= E[(\mathbf{M}_j - \mu_j)^2 / \sigma_j^2] = \sigma_j^2 / \sigma_j^2 = 1.0$$

Therefore, by application of this simple algebraic transformation, the maximum value ratios between all $\mathbf{M}_j^N$ vectors are mapped into a common interval and can be summed with each other. To generate the MDWM, all $\mathbf{M}_j^N$ vectors are superimposed as indicated below

$$M_{GI}(k) = \sum_j M_j^N(k),$$

$$j = H, \ dfI, \ dfII, \ CL, \ AR, \ MS \qquad (22)$$

In Fig. 3, an example of the $M_j^N(k)$, $j = H, dfI, dfII, CL, AR, MS$ and the calculated MDWM obtained from an arbitrary holter data is shown. As a summary of all aforementioned parts, the MDWM reacts in edges, maximum (minimum) slope locations and maximum (minimum) elevation locations therefore, this quantity is a suitable decision statistic to detect edges and extremums of an excerpted segment in the analysis window. In the MDWM, several geometric parameters such as maximum value to minimum value ratio, area, extent of smoothness or being impulsive and distribution asymmetry can be found, (see Fig. 3). The capacities of the MDWM -based detection-delineation algorithm are shown in the next sections.

2.3 Detection of QRS Complexes via α-Level Neyman-Pearson Based Classifier
2.3.1 Design of False Alarm Probability (FAP) - Bounded Classifier

In this study, in order to detect QRS complexes via segmentation of the MDWM, α-Level Neyman-Pearson which is of controlled false alarm probability (FAP) is designed by implementation of Gaussian (normal) stochastic structure.

In order to cast the detection of QRS complexes into a probabilistic framework, suppose that the observation set $\{Z = z \mid Z \in \Omega, \Omega = \Gamma_0 \cup \Gamma_1\}$ consists of two states of nature *Hypo.* 0 and *Hypo.* 1, i.e., the samples of observation (in this study observation set is MDWM) samples Z=z are distributed according to two probability density functions (pdf) $p_0(z)$ and $p_1(z)$. The structure of the hypotheses *Hypo.* 0 and *Hypo.* 1 is shown in Eq. 23, in which A_0 and A_1 are the parameters of the hypothesis test problem and N is a stationary stochastic process with the corresponding model and parameters.

$$\begin{cases} \text{Hypo.0}: \ Z = N + A_0 \\ \text{Hypo.1}: \ Z = N + A_1 \end{cases}, \ A_1 > A_0 \quad (23)$$

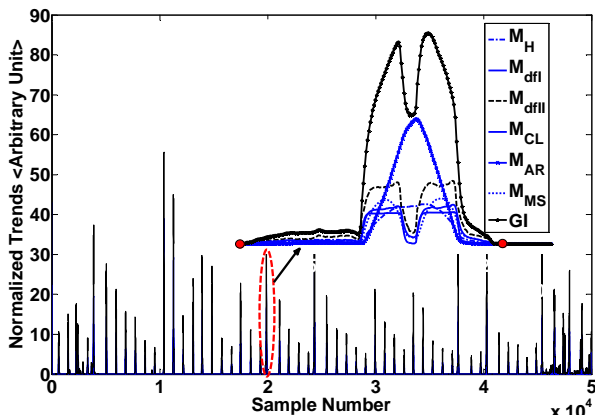In this study, it is supposed that N is a Gaussian zero mean stationary process with standard deviation σ.

Fig.3 Obtained normalized $M_j^N(k)$, j = H, dfI, dfII, CL, AR, MS

and the resulted MDWM to illustrate the behavior of each measure.

Therefore the pdf of observation under states of nature Hypo. 0 and Hypo. 1 ($p_0(z)$ and $p_1(z)$ respectively) is according to the following equation

$$\begin{cases} p_0(z) = \dfrac{1}{\sqrt{2\pi}\sigma} \exp\left[\dfrac{-1}{2\sigma^2}(z - A_0)^2\right] \\ p_1(z) = \dfrac{1}{\sqrt{2\pi}\sigma} \exp\left[\dfrac{-1}{2\sigma^2}(z - A_1)^2\right] \end{cases} \quad (24)$$

In order to construct a FAP controlled Neyman-Pearson classifier, the likelihood ratio (LR) which is the ratio between Hypo. 1 and Hypo. 0 pdfs, should be obtained as follows

$$L(z) = \frac{p_1(z)}{p_0(z)} = \frac{\dfrac{1}{\sqrt{2\pi}\sigma} \exp\left[\dfrac{-1}{2\sigma^2}(z - A_1)^2\right]}{\dfrac{1}{\sqrt{2\pi}\sigma} \exp\left[\dfrac{-1}{2\sigma^2}(z - A_0)^2\right]}$$

$$= \exp\left[\frac{-1}{2\sigma^2}(z - A_1)^2 + \frac{+1}{2\sigma^2}(z - A_0)^2\right] \quad (25)$$

By taking log(.) (natural logarithm) from the obtained LR (the resulted ratio is consequently called log-LR), and solving the inequality $\log(L(z)) > \tau$ for finding the equivalent inequality for z, the following result is obtained

$$\log(L(z)) =$$
$$\frac{+1}{2\sigma^2}\left[(z - A_0)^2 - (z - A_1)^2\right]$$
$$\log(L(z)) > \tau \Rightarrow \frac{+1}{2\sigma^2}\left[(z - A_0)^2 - (z - A_1)^2\right] > \quad (26)$$
$$\Rightarrow z > \tau'$$

According to Eq. 26, if $z > \tau'$, where τ' is a threshold that is determined according to FAP value and the other test parameters, then z will belong to class *Hypo.* 1. The FAP of this test is the integration of pdf $p_0(z)$ over the Γ_1 ($z > \tau'$) region as follows

$$\text{FAP} = P_0(\Gamma_1) = \int_{\tau'}^{+\infty} p_0(z)\,dz$$
$$= \int_{\tau'}^{+\infty} \frac{1}{\sqrt{2\pi}\sigma} \exp\left[\frac{-1}{2\sigma^2}(z - A_0)^2\right]dz \quad (27)$$
$$= 1 - \Phi\left(\frac{\tau' - A_0}{\sigma}\right)$$

where $\Phi(x)$ is the unit variance and zero mean Gaussian cumulative probability function with the following integral definition

$$\Phi(x) = \frac{1}{\sqrt{2\pi}} \int_{-\infty}^{x} e^{\frac{-1}{2}t^2}\,dt \quad (28)$$

By equaling the latest term of Eq. 27 to the given FAP value α and by solving it to find the threshold τ'

as a function of A_0, σ and α, the following result is obtained

$$1 - \Phi\left(\frac{\tau' - A_0}{\sigma}\right) = \alpha \qquad (29)$$

$$\tau' = A_0 + \sigma\Phi^{-1}(1-\alpha) \qquad (30)$$

where α represents the level (false-alarm probability) of the binary Neyman-Pearson radius test and is chosen as $0.005 \leq \alpha \leq 0.05$, [34]. It should be noted that although Eqs. 24 to 30 were derived based on simplifying assumptions (independent samples, identical distribution, etc.); however, similar to derivation of Kalman filtering equations, its operation depends only on the first and second-order moments of the signal. Consequently, it can be easily implemented in actual cases and a high performance would be resulted from the algorithm in practical applications, [34]. The parameters A_0 and σ are the test parameters and should be determined properly to achieve acceptable results. In order to find A_0, according to Fig. 4, first, histogram (discrete probability distribution function) of the MDWM is estimated using an existing simple method [31] and then the maximum value of the obtained histogram is assigned as A_0. In other words, A_0 is the maximum distribution (or equivalently A_0 is the value of the MDWM baseline). As shown in Fig. 4, σ is the distance between A_0 value and the first corner of histogram taking place immediately after A_0. It should be noted that histogram estimation can be fulfilled recursively (on-line) or cumulatively (off-line). The accuracy of the second method is higher than the on-line methods but in the expense heavier computational burden as well as missing real-time implementation of the method. More details relating this section is omitted and left to be seen in [33-34].

A large M_{CL} value of a signal points out a sharp ascending or descending regime and consequently, this
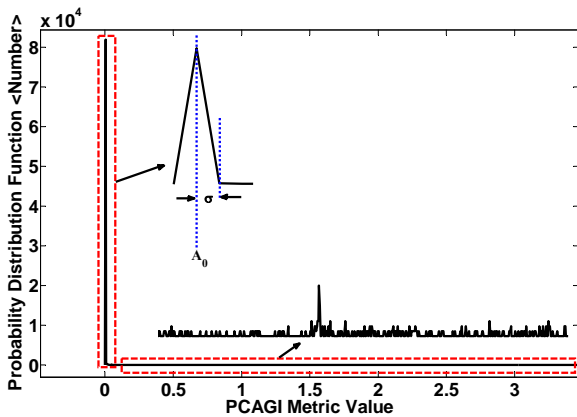
Fig. 4 Determination of α-level Neyman-Pearson classifier parameters via estimation of the MDWM histogram (discrete probability distribution function). The depicted histogram is obtained from an arbitrary high-resolution holter data.

quantity make the MDWM sensitive to the high-slope parts of the signal in the analysis window, either ascending or descending. Generally, the M_{CL} measure indicates the extent of flatness (smoothness or impulsive peaks) of samples in the analysis window. This measure allows detecting sharp ascending/descending regimes occurred in the excerpted segment, [31, 32].

3 Databases, Results and Evaluation of the MDWM-Based ECG Events Detection-Delineation Algorithm

3.1 Technical Descriptions of Employed Databases
3.1.1 The MIT-BIH Arrhythmia Database
The MIT-BIH Arrhythmia Database contains 48 half-hour excerpts of two-channel ambulatory ECG recordings, obtained from 47 subjects studied by the BIH Arrhythmia Laboratory. Twenty-three recordings were chosen at random from a set of 4000 24-hour ambulatory ECG recordings collected from a mixed population of inpatients (about 60%) and outpatients (about 40%) at Boston Hospital; the remaining 25 recordings were selected from the same set to include less common but clinically significant arrhythmias that would not be well-represented in a small random sample. The recordings were digitized at 360 samples per second per channel with 11-bit resolution over a 10 mV range. Two or more cardiologists independently annotated each record; disagreements were resolved to obtain the computer-readable reference annotations for each beat (approximately 110,000 annotations in all) included with the database, [20].

3.1.2 The TWA Database
This database has been assembled for the PhysioNet/Computers in Cardiology Challenge 2008. It contains 100 multichannel ECG records sampled at 500 Hz with 16 bit resolution over a $\pm$ 32 mV range. The subjects include patients with myocardial infarctions, transient ischemia, ventricular tachyarrhythmias, and other risk factors for sudden cardiac death, as well as healthy controls and synthetic cases with calibrated amounts of T-wave Alternans, [23].

3.1.3 The QT Database
The QT Database includes ECGs which were chosen to represent a wide variety of QRS and ST-T morphologies, in order to challenge QT detection algorithms with real-world variability. The records were chosen primarily from among existing ECG databases, including the MIT-BIH Arrhythmia Database, the European Society of Cardiology ST-T Database, and several other ECG databases collected at Boston's Medical Center. All records were sampled at 250 Hz, [21]. Those which were not originally sampled at that rate were converted using the MIT Waveform Database Software Package, [24].

3.1.4 High Resolution DAY General Hospital Database

The high-resolution holter database of DAY hospital contains 24-hour 3-lead records of about 150 patients including diverse ECG arrhythmias such as BBB, PVC, PAC, myocardial infarction, heart failure, ischemia and T-wave alternans. The sampling frequency of this database is 1000 Hz with 32-bits of resolution [16]. The electrodes of each holter are attached to the subjects chest skin surface at positions 1, 3, 5 via suitable vacuum cups.

3.2 Procedure of the Proposed MDWM -Based ECG Waves Detection-Delineation Algorithm
3.2.1 Bandpass FIR Filtering to Remove Noise and Motion Artifacts

General block diagram of multi-lead based ECG events detection-delineation algorithm is illustrated in Fig. 5. According to this flow-chart, first three lead high resolution 24 hour holter ECG signals are extracted and using a bandpass FIR filter with (0.40~40) Hz passband characteristic, each lead is filtered to remove contaminating effects such as baseline wander, motion artifacts and high frequency measurement noise. It can be stated that the main components of the ECG signal relating to the heart electrical activity, have frequency specifications with the uttermost concentration on the (0.40~40) Hz interval, [16].

3.2.2 Application of à Trous Discrete Wavelet Transform

In this step, using à trous discrete wavelet transform algorithm, appropriate scales 2^λ ($\lambda=1,2,\ldots,6$) are extracted from the resulted norm. In order to amplify the effects of important events of the ECG signal such as P-wave, T-wave and QRS complex and also to weaken disturbing effects to the possible extent, for each lead j ($j = V_1, V_2, V_3$), a synthetic quantity is extracted from scales 2^λ ($\lambda=3,\ldots,6$) as follows

$$W_{S,j}[n] = \sum_{\lambda=3}^{6} W_{2^\lambda}^{j}[n]\, W_{2^2}^{j}[n]$$

$$n = 1, 2, \ldots, N, j = V_1, V_2, V_3 \tag{31}$$

In order to increase the robustness of the MDWM -based detection-delineation algorithm, after appropriate noise and baseline wander removal from each lead, the Euclidean norm between samples of $W_{S,j}[n]$, $j = V_1, V_2, V_3$ is calculated as

$$W_T[n] = \sqrt{W_{S,1}^2[n] + W_{S,2}^2[n] + W_{S,3}^2[n]}$$

$$n = 1, 2, \ldots, N \tag{32}$$

As it will be shown, by application of this norm instead of an single individual lead, when a lead contains transient or even permanent disturbances, other clean leads compensate the lack of information caused by the noisy lead and consequently the algorithm shows more endurance against probable noise and motion artifacts.

3.2.3 Resampling of the Obtained Synthetic Scale into a Target Frequency (Unified Parameters Adjustment)

It should be noted that almost all parameters of the proposed detection delineation algorithms [11,13,16,17] are highly dependent to the sampling frequency of the holter systems. For example, sampling frequencies 128 Hz, 250 Hz, 500 Hz, 750 Hz, 1 kHz, 2 kHz and 10 kHz can be seen among holter based databases [35]. In order to introduce a unified ECG individual events detection framework which is applicable for all sampling frequencies, after calculation of the synthetic scale as described previously, the original signal in the core sampling frequency is mapped to a new trend with target sampling frequency 750 Hz. By this operation, once the parameters of the algorithm are properly regulated for the target sampling frequency, the algorithm can be implemented to the holter data sampled with any rate.

3.2.4 MDWM Generation and Normalization

A window with the length of L ~ (40-50 msec) samples is then slid sample to sample on the resampled version of signal $W_T[n]$ and the measure MDWM is calculated in each window (see section B.2.7).
In the next step, the obtained trend MDWM is normalized. Normalization of the signal MDWM is an algebraic linear transformation that maps the signal MDWM so as its first and second moments are transferred to zero and unity respectively, i.e.,

$$(MDWN)_N =$$
$$[MDWN - mean(MDWN)]/std(MDWN) \tag{33}$$
$$mean\big[(MDWN)_N\big] = 0 \,;\; std\big[(MDWN)_N\big] = 1.0$$

where $mean(\cdot)$ and $std(\cdot)$ are mean value and standard deviation operators, respectively. The aim of normalization is to diminish subject dependency of the signal MDWM if so, once applied thresholds and decision criteria are tuned; their performance is preserved during application of the method to any subject [13].

3.3 Detection and Delineation of Holter ECG Events
3.3.1 Detection and Delineation of the QRS Complexes (Normal, Ectopy)

According to Eq. 30 of section B.3.1, after determination of the test parameters A_0 and σ using histogram estimation and given FAP α, the threshold τ' is determined and used to segment the MDWM into QRS (hypo. 1) and non-QRS (hypo. 0) regions. The decision function $\delta(n)$ is then obtained with the following structure

$$\delta_{MDWM}(n) = \begin{cases} QRS\ Complex & MDWM(n) \geq \tau' \\ non-QRS\ Complex & MDWM(n) < \tau' \end{cases} \tag{34}$$
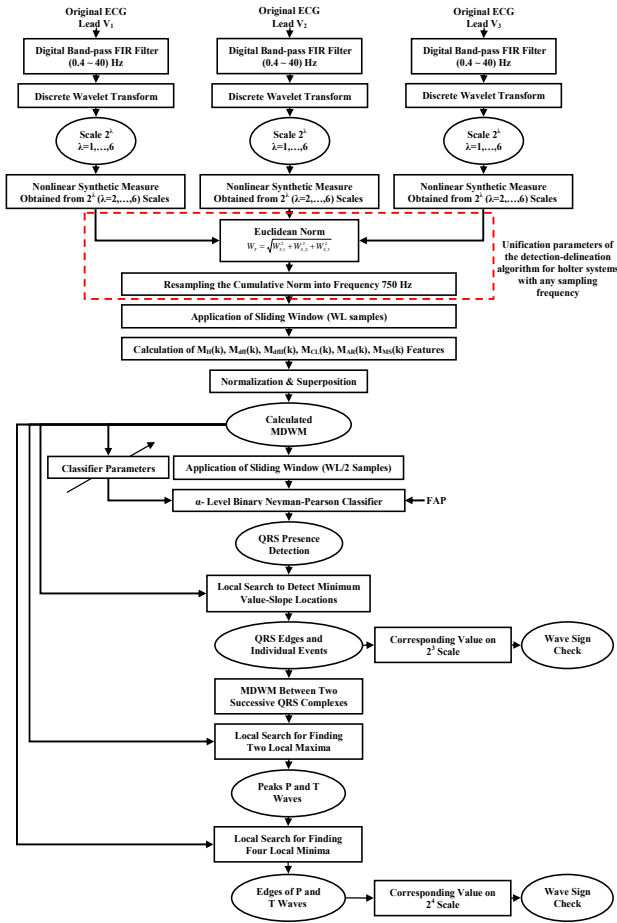
Fig. 5 General block diagram of the proposed ECG events (P-wave, QRS complex and T-wave) detection-delineation algorithm based on analysis of multi-lead obtained MDWM.

To this end, first all samples of the MDWM signal is analyzed via decision rule presented by Eq. 34 and the edges of each obtained rectangular pulse is determined using appropriate calculations and are assigned as the edges of the detected QRS complex, (see Fig. 6). These points are then transferred to the 2^3 scale and the index for extremum values are specified between edges. If the minimum is occurred before the maximum, a dominant local minimum value would exist in the original signal and vice versa. In this way, the sign of the QRS complex (upward or downward) can be realized. In order to detect Q and S waves, the mean value of the index corresponding to the number of crossings of zero is calculated for movement between R-wave and right and left edges.

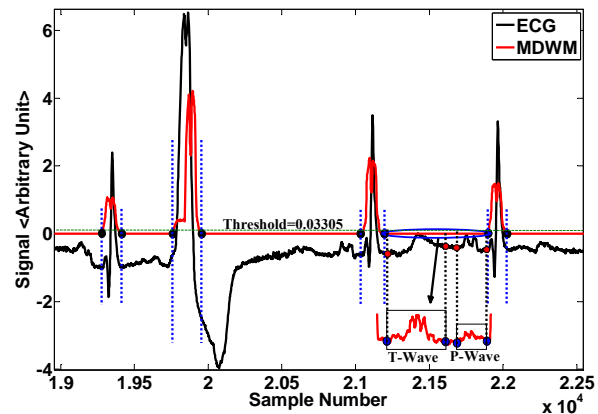### 3.3.2 Detection and Delineation of P and T Waves (Normal, Biphasic, Inverted)

In order to detect P and T waves, a local search for two local maxima is conducted between two successive extremum values in the MDWM signal. The local maximum close to the right R-wave is specified as P-wave index and the one close to the left R-wave is

specified as T-wave index of the preceding beat. In the next step, in order to determine the onset and offset of P and T-waves, a segment of the signal MDWM between two consequent QRS complexes is chosen and a local search is conducted to find four local minima, as follows

a) A search between the end of the preceding QRS complex and T-wave peak (beginning of the preceding T-wave)

b) A search between the T-wave peak and half of RR interval (end of the preceding T-wave)

c) A search between the half of the RR interval and the P-wave peak (beginning of P-wave)

d) A search between the P-wave peak and the beginning of the next QRS complex (the end of P-wave)

Generally, detection and delineation of T-wave is more difficult than P-wave. Therefore, the most significant part of the error corresponding to waves detection is related to T-wave. The block diagram of the algorithm for the detection and delineation of QRS complex, P-wave and T-wave is illustrated in Fig. 6. Examples of QRS, P-wave and T-wave detection and delineation are depicted in Figs. 7-10. In these figures, solid circles represent the wave edges (beginning and end), solid triangles show the extremums of the waves and solid squares marks the offset of the detected events.

Detection and delineation of P and T-waves are described in more detail. First of all, two successive QRS complexes are detected and the corresponding edges are delineated using the MDWM measure. Next, the distance between the MDWM of the corresponding wavelet transform of the right edge of the first complex and the left edge of the second complex is determined.

Fig. 6 An example of α-level Neyman-Pearson based detected-delineated P-wave, QRS complex and T-wave of high resolution ambulatory holter ECG via segmentation of MDWM measure. (Detection-delineation of normal QRS complexes, delineation of a PVC complex, and delineation of T and P waves).
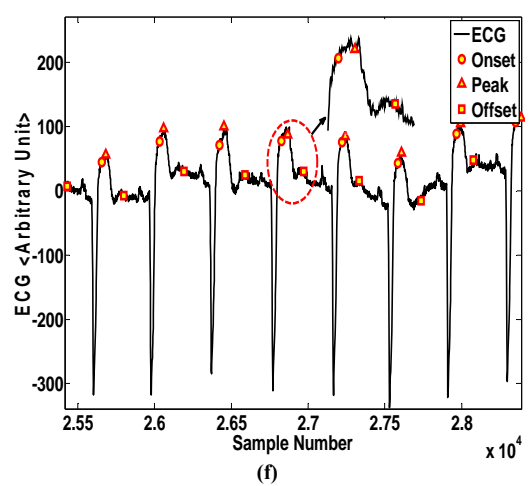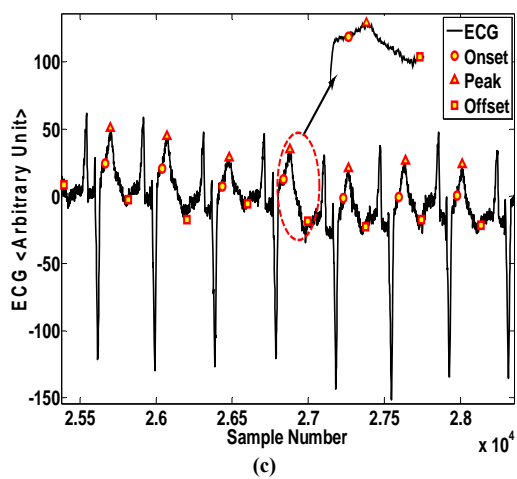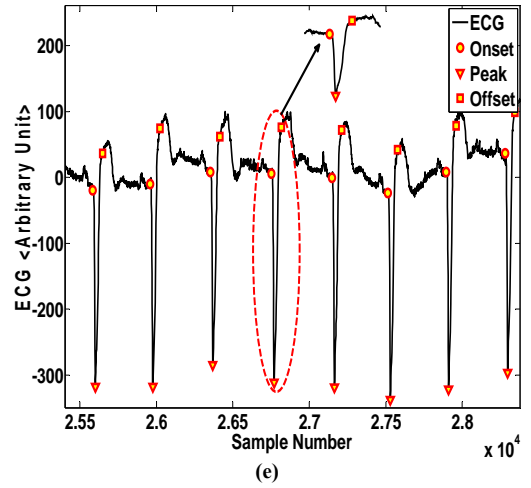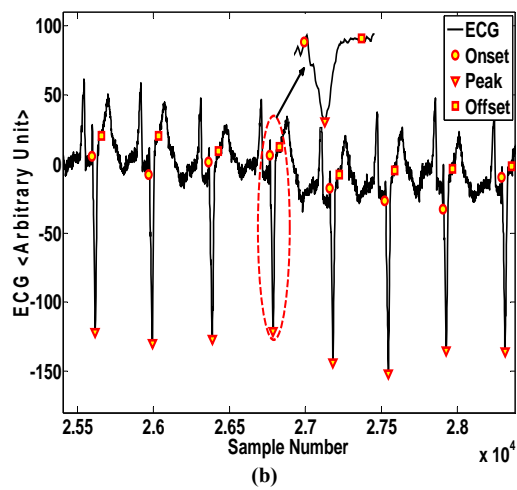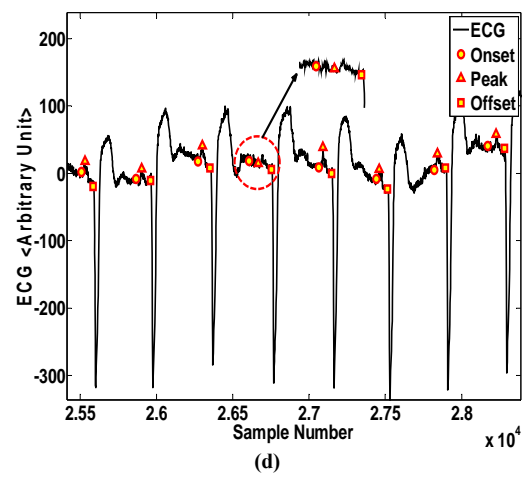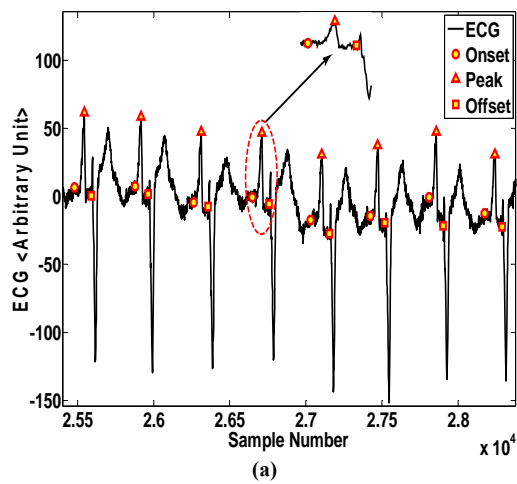
Fig. 7 An excerpted segment from total delineated from lead I (left) of record # 108 MITDB ECG. Delineated (a) P-waves, (b) QRS complexes and (c) T-waves. Lead II (right) of record # 108 MITDB ECG. Delineated (d) P-waves, (e) QRS complexes and (f) T-waves. (Circles: edges of event, Triangles: Peak of events).
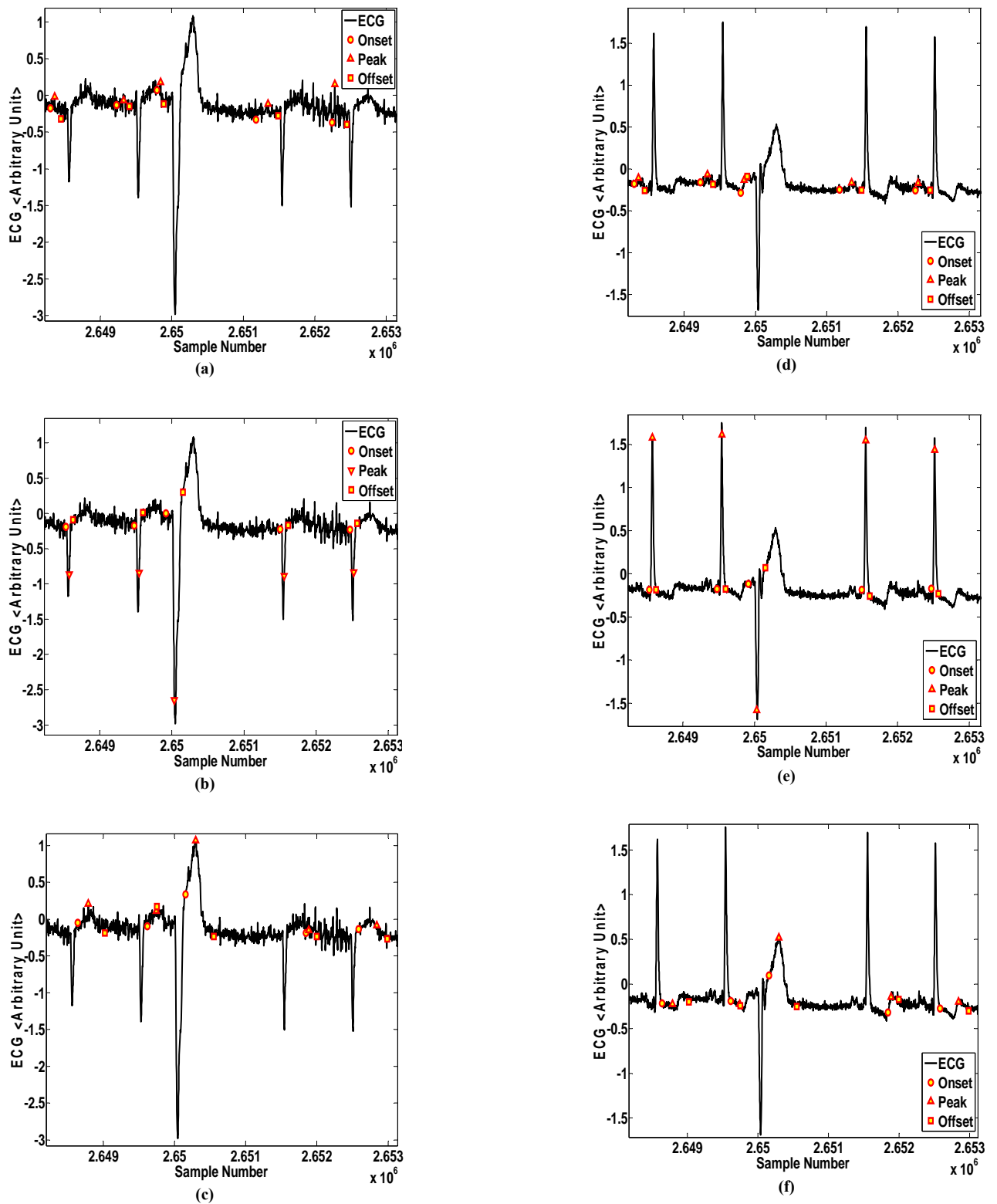
Fig. 8 Two leads detected-delineated trends of a high resolution holter ECG including a PVC with full compensatory pause (FCP). An excerpted segment from total delineated from lead V$_1$ (left) of an arbitrary holter ECG. Delineated (a) P-waves, (b) QRS complexes and (c) T-waves. Lead V$_2$ (right) delineated (d) P-waves, (e) QRS complexes and (f) T-waves. (Circles: edges of event, Triangles: Peak of events).
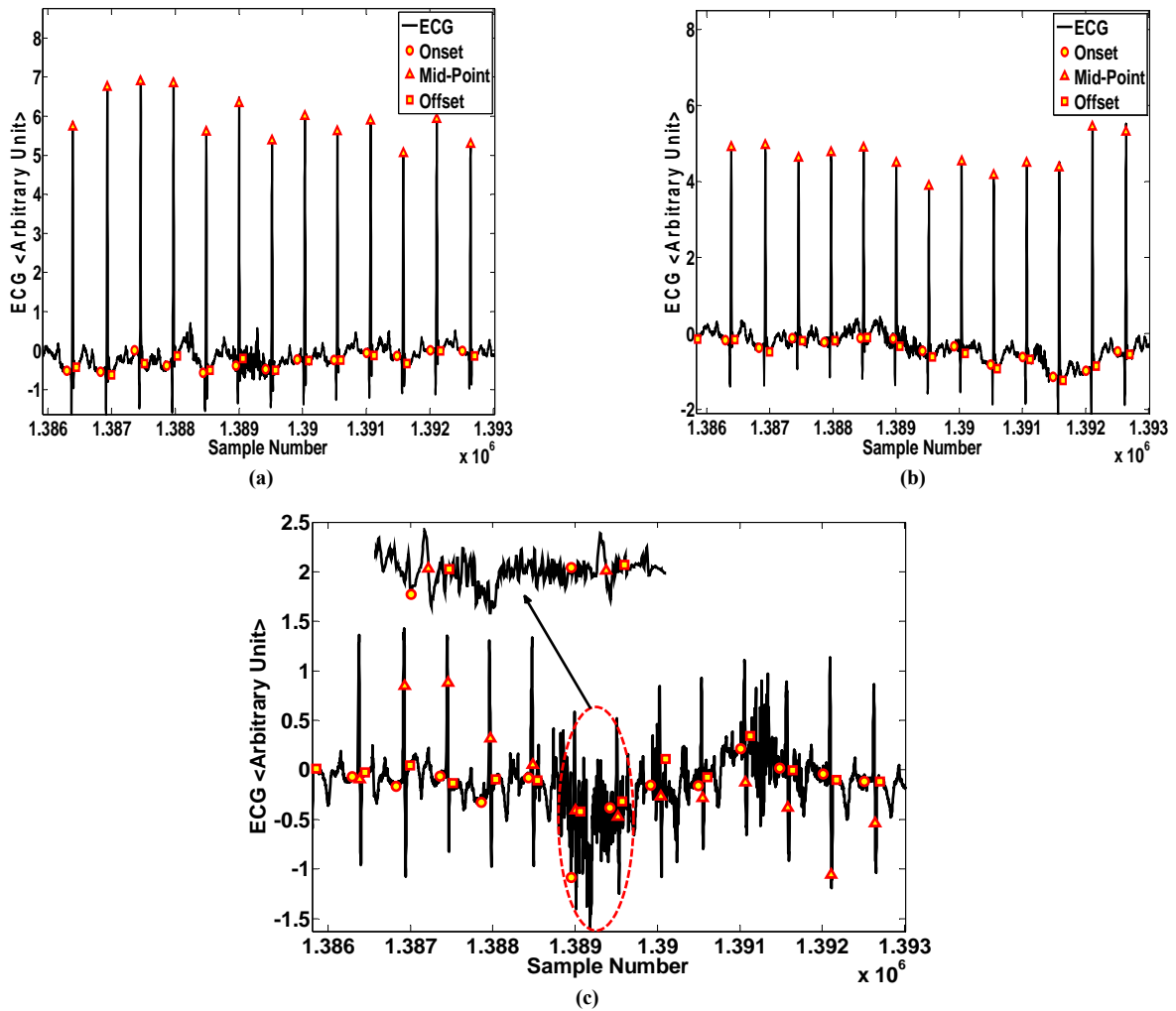
Fig. 9 Three leads detected-delineated trends obtained from a high resolution ambulatory holter record. (a) Lead V_1, (b) Lead V_2, and (c) Lead V_3. Although SNR value in some QRS complexes of the third lead is lower than the corresponding ones in other leads, the probable errors is eschewed by compensation of the information lack by the other leads.

The RR interval is then divided into two sections. Because the MDWM measure is strictly positive, one dominant maximum will be found in each of these two intervals. Finally, a local search is conducted to the left and right of each of these maxima, and the position where MDWM slope is less than 1/15 to 1/20 of the maximum slope in the window is identified as wave edge. The following conditions are observed;

- If a T-wave and a P-wave exists in the RR interval, they will be detected regardless of their sign, i. e., positive, negative or biphasic. (Waves sign is determined based on the sign of the corresponding wavelet transform)

- If there is only a T-wave in the RR interval, the left edge and the maximum amplitude of this wave will be easily detected. However, there may be some problems in finding the right edge. In this case, a new algorithm is required for the determination of the P-wave power.

- If there is no P or T wave in the RR interval, it will be accurately announced by the algorithm.

As mentioned above, one of the merits of the presented algorithm is that the sign of P or T-wave and their morphology will not affect the performance of the algorithm.

In Fig. 11, some arrhythmic cases encountered during detection-delineation are shown. Fig. 11-a shows a PAC complex of delayed sinus node reset type. In Fig. 11-b, some normal complexes pursued by a PVC of retrograde conduction into atrium type. In Fig. 11-c, an ECG trend with multi-focal PVCs including BBB arrhythmia is shown. In this figure, first PVC complex is of retrograde conduction into atrium type while the second PVC is a full compensatory pause complex.
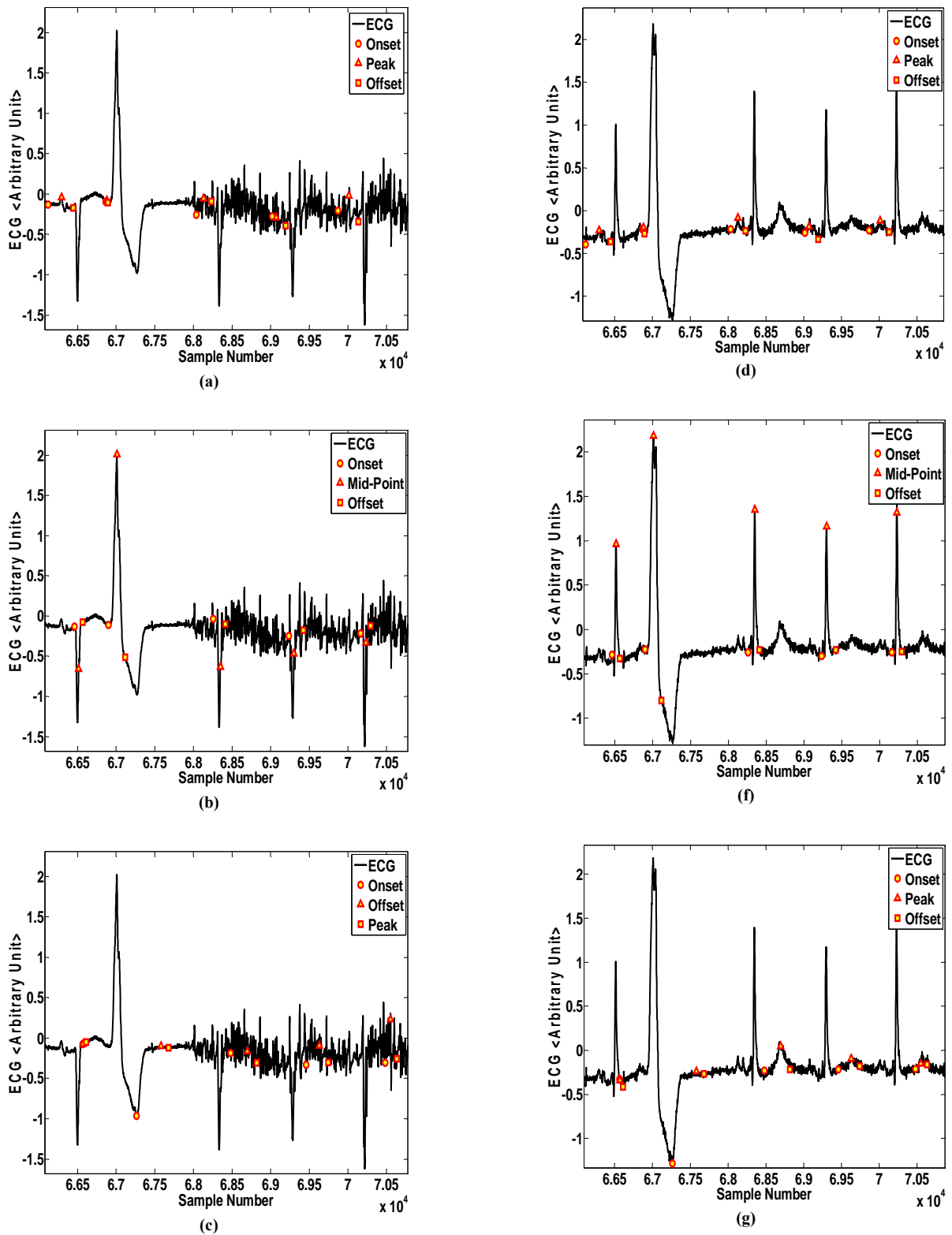
Fig. 10 Two leads detected-delineated trends of a high resolution holter ECG including a PVC with retrograde conduction into atrium (RCA). An excerpted segment from total delineated from lead V_1 (left) of an arbitrary holter ECG. Delineated (a) P-waves, (b) QRS complexes and (c) T-waves. Lead V_2 (right) delineated (d) P-waves, (e) QRS complexes and (f) T-waves. (Circles: edges of event, Triangles: Peak of events). This figure shows qualitatively the robustness of the presented algorithm against low SNR in a lead.

3.4 Validation of the Presented Algorithm

Numerous databases with different sampling frequencies and signal to noise ratio are used in this study to validate the performance of the proposed detection algorithm. To validate the QRS detection and delineation algorithm, MITDB (F_s=360Hz), TWADB (F_s=500Hz), and QTDB (F_s=250Hz) which contain annotation files are used (CHECK#0). It should be noticed that in challenging cases, results were delivered
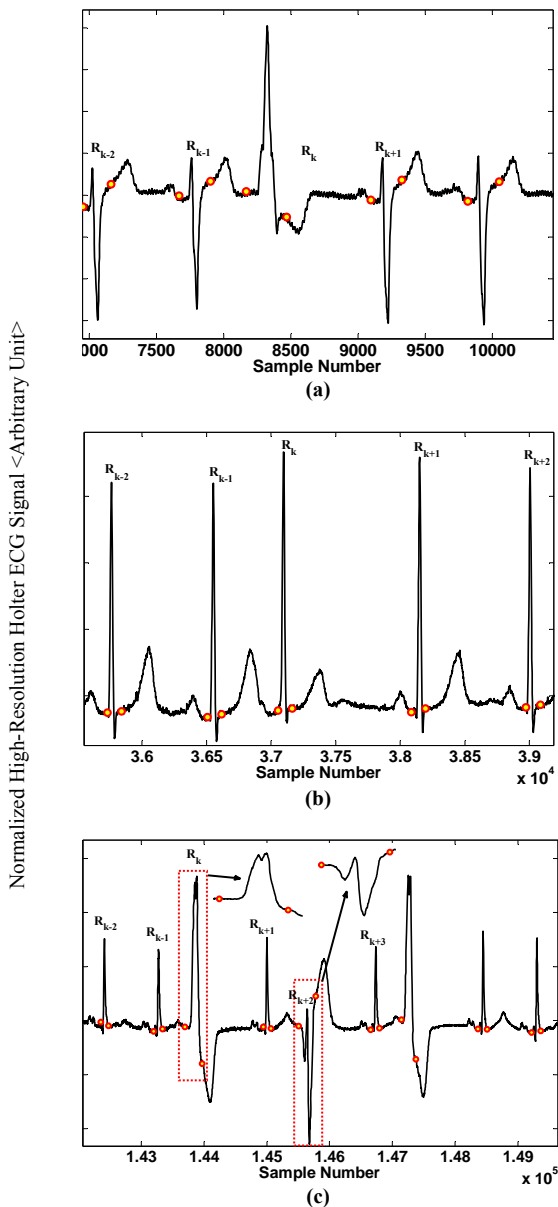
Fig. 11 A delineated high resolution holter ECG trend including normal complexes and (a) a PVC with a retrograde conduction into atrium (RCA) (Rk Rk+1 > Rk-2 Rk-1), (b) a PAC with delayed sinus node reset (Rk Rk+1 > Rk-2 Rk-1) (c) normal complexes and some BBBs beats pursued by a PVC with a retrograde conduction into atrium (RCA). The second PVC is a full compensatory pause (FCP) complex (R_{k+1} R_{k+3} =2 R_{k-2} R_{k-1}), the unit of these figures are arbitrary.

to the cardiologist and accordingly the detection algorithm was re-validated (CHECK#1). In cases of QRS with very abnormal morphologies, the results were also checked by some residents (CHECK#2).

Many approaches have yet been developed in the area of wave detection which are all applied only to the Lead I. Thus, in order to validate the performance of the proposed detection algorithm, it was applied to Lead I. If so, it would be possible to compare the presented algorithm with other researches. MITDB, QTDB and TWADB include 48, 105 and 100 subjects respectively. All these data were converted to MAT-files using the WFDB Software [24].

The presented detection algorithm was validated in a sequential order in three steps:

Detection of QRS Complexes: in order to detect QRS complexes, the presented algorithm was applied to all MITDB, QTDB, EDB and TWADB signals and the results of QRS detection and annotation files were compared in a computer program (CHECK#0). These results were then delivered to cardiologist in graphical format (such as Figs. 6, 7) and accordingly the detection algorithm was modified (CHECK#1). Due to the fact that a universally accepted gold standard exists in the area of QRS detection, validation procedure was significantly simplified to the step CHECK#0. The results of this study are presented in Tables 1, 2 and 3 to be compared to other works. As two instances, record #108 includes 1824 annotated complexes which was a mixture of normal complexes, PVCs and blocked PACs. After applying the presented algorithm to this record, the statistical values of FP = 3, FN = 4, and were finally achieved which yield to the values of Se = 99.72% and P+ = 99.88%, respectively. Record #207 includes 2385 annotated complexes which are a mixture of normal complexes and ventricular Flutter. In the next step, for the results of the algorithm to be compared with those of Martinez et al, the VF beats were eliminated. The presented algorithm was applied to this record and the statistical values of FP = 4, FN = 8, and were achieved which yield to the values of Se = 99.60% and P+ = 99.72%, respectively.

1. Delineation of QRS Complexes, P and T-Waves: In comparison to QRS detection, the delineation of QRS complexes and P and T-waves is a rather complicated approach. QTDB includes 105 files with the sampling frequency of 250 Hz containing beginning, end and peak of P-wave and QRS complex as well as the peak and end of the T-wave in the corresponding annotation files. Using this information, it would be possible to completely detect and delineate P-waves and detect the beginning and end of QRS complexes (CHECK#0, CHECK#1). Also, it is possible to detect the peak and end of the T-wave using QTDB. Nonetheless, detection of all waves in the QRS complex and the beginning of T-wave

using these two databases is not possible. To meet this end, the CHECK#1 and CHECK#2 approaches were implemented. The results of delineation of P-wave, detection of QRS edges, and detection of the end and peak of the P-wave using the QTDB are presented in Table 4. In this table, sensitivity percentage, positive predictivity percentage and minimum-maximum location error in milliseconds are presented.

Accordingly, it should be noticed that a higher sensitivity and positive predictivity was obtained in this study in comparison to other researches due to applying multi-lead features analysis. Also, developing the MDWM -based measure lead to a significant decrease in the error related to edges detection. One of the objectives of this study is to evaluate the robustness of the presented detection algorithm versus the measurement noises and artifacts so the method is applied to several databases.

2. As final step in the validation of the proposed algorithm, it was applied to 3-lead Holter data of 4 subjects (1 hour long) and the results of application of the CHECK#1 and CHECK#2 are presented in Table 5.

It should be noted that because the proposed algorithm accurately detects J-points and the beginning of the T-wave, using the CHECK#2 approach it was realized that the presented algorithm has acceptable performance in the determination of late potentials. In Fig. 12, a sample delineated high resolution holter ECG with an estimate of late potential is shown. It should be noted that during myocytes refractory phase, the potential difference between beginning of T-wave and J-point of corresponding QRS complex is called late potential, [1].

As the final step of the accuracy performance checking, in each case the trend of RR-tachogram is obtained and plotted. It should be noted that if RR-interval is remarkably less than the mean value, probable false positive (FP) error may exist. On the other hand, if RR-interval is significantly greater than the mean value, the false negative error may probably exist. In Fig. 13, two examples of RR-tachogram obtained from holter data of two patients of hospital including PVC and PAC beats are shown.

In table 6, some specifications of ECG events detection-delineation are shown. According to this table, the presented detection-delineation algorithm possesses the best performance characteristics namely as speed of processing, accuracy and robustness against noise and motion artifacts.
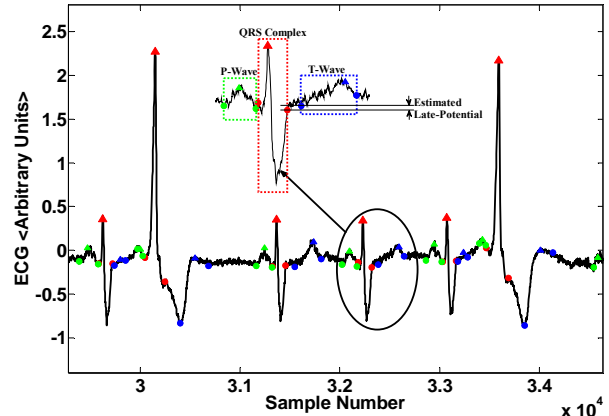

Fig. 12 A delineated high resolution holter ECG trend and illustration of the late potential estimation.
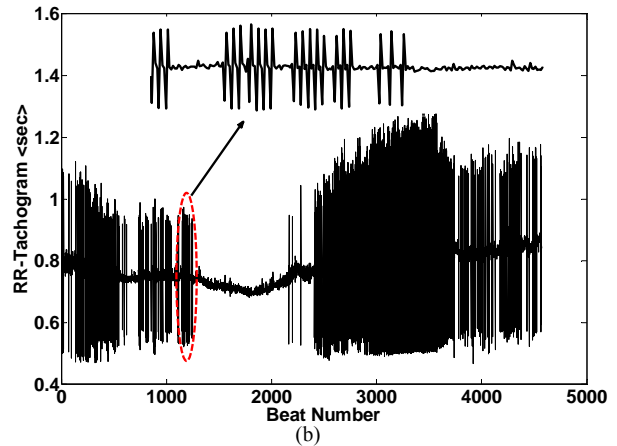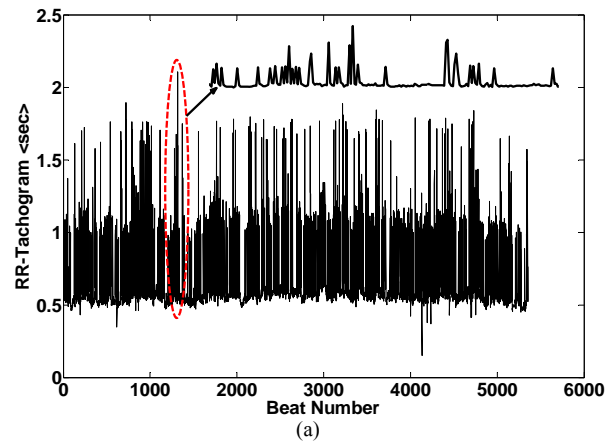

Fig. 13 The detected RR-tachogram to estimate the number of FP and FN type errors; (a) this trend shows a FP error during the PAC-induced heart rate turbulence, (b) a trend with no FP and FN errors during the PVC-BBB induced heart rate turbulence.

Table 1 Performance evaluation of several QRS detection algorithms: Application to MITDB.

Detection Algorithm	# of Annotations	TP	FP	FN	Error (%)	Se (%)	P+(%)
This Study	109428	109375	81	53	0.12	99.95	99.93
Ghaffari et al. [13]	109428	109367	89	61	0.14	99.94	99.91
Ghaffari et al. [16]	109428	109327	129	101	0.21	99.91	99.88
Ghaffari et al. [11]	109428	109215	160	213	0.34	99.80	99.85
Martinez et al. [15]	109428	109208	153	220	0.34	99.80	99.86
Li et al. [25]	104182	104070	65	112	0.17	99.89*	99.94*
Hamilton et al. [26]	109267	108927	248	340	0.54	99.69	99.77
Pan et al. [27]	109809	109532	507	277	0.71	99.75	99.54
Moody et al. [28]	109428	107567	94	1861	1.79	98.30	99.91

* In this case, a discrepancy is found between the published result and the review paper [10].

Table 2 Performance evaluation of QRS detection algorithms: Application to QTDB.

Detection Algorithm	# of Annotations	TP	FP	FN	Error (%)	Se (%)	P+(%)
This Study	86892	86869	61	23	0.10	99.97	99.93
Ghaffari et al. [13]	86892	86854	70	38	0.12	99.96	99.92
Ghaffari et al. [16]	86892	86845	79	47	0.15	99.94	99.91
Ghaffari et al. [11]	86892	86819	94	73	0.19	99.92	99.89
Martinez et al. [15]	86892	86824	107	68	0.20	99.92	99.88
Moody et al. [28]	86892	84458	459	2434	3.33	97.2	99.46

Table 3 Performance evaluation of QRS detection algorithms: Application to TWADB.

Detection Algorithm	# of Annotations	TP	FP	FN	Error (%)	Se (%)	P+ (%)
This Study	11789	11784	7	5	0.11	99.96	99.94
Ghaffari et al. [13]	11789	11782	11	7	0.15	99.94	99.91
Ghaffari et al. [16]	11789	11776	18	13	0.26	99.89	99.84
Ghaffari et al. [11]	11789	11760	24	29	0.45	99.75	99.80

Table 4 Performance evaluation of delineation algorithms on QTDB, (NR: Not Reported, NA: Not Applicable, LE: Location Error).

Method	Accuracy Parameters	P_{ON}	P_{peak}	P_{OFF}	QRS_{ON}	QRS_{peak}	QRS_{OFF}	T_{ON}	T_{peak}	T_{OFF}
This Study	Se (%)	99.69	99.69	99.69	99.97	99.97	99.97	99.93	99.93	99.93
	P+ (%)	99.21	99.21	99.21	99.95	99.95	99.95	99.92	99.92	99.92
	LE ($\mu\pm\sigma$) (msec)	-1.1±3.4	3.4±6.3	-0.1±3.1	-0.6±3.3	0.7±1.9	-0.1±5.4	-1.0±3.7	-0.2±2.6	-0.1±5.2
Ghaffari et al. [13]	Se (%)	99.64	99.64	99.64	99.97	99.97	99.97	99.93	99.93	99.93
	P+ (%)	99.00	99.00	99.00	99.95	99.95	99.95	99.92	99.92	99.92
	LE ($\mu\pm\sigma$) (msec)	-1.1±4.7	3.6±7.7	-0.2±3.4	-0.6±4.9	0.7±2.4	-0.1±5.9	-1.1±4.1	-0.2±3.1	-0.1±6.8
Ghaffari et al. [16]	Se (%)	99.46	99.46	99.46	99.94	99.94	99.94	99.87	99.87	99.87
	P+ (%)	98.83	98.83	98.83	99.91	99.91	99.91	99.80	99.80	99.80
	LE ($\mu\pm\sigma$) (msec)	-1.2±6.3	4.1±10.5	0.7±6.8	-0.6±8.0	1.1±2.8	0.3±8.8	-1.4±5.7	0.3±4.1	0.8±10.9
Martinez et al. [15]	Se (%)	98.87	98.87	98.75	99.97	NR	99.97	NR	99.77	99.77
	P+ (%)	91.03	91.03	91.03	NA	NR	NA	NR	97.79	97.79
	LE ($\mu\pm\sigma$) (msec)	2.0±14.8	3.6±13.2	1.9±12.8	4.6±7.7	NR	0.8±8.7	NR	0.2±13.9	-1.6±18.1
Laguna et al. [29]	Se (%)	97.7	97.7	97.7	99.92	NR	99.92	NR	99.0	99.0
	P+ (%)	91.17	91.17	91.17	99.91	NR	NA	NR	97.74	97.71
	LE ($\mu\pm\sigma$) (msec)	14.0±13.3	4.8±10.6	-0.1±12.3	-3.6±8.6	NR	-1.1±8.3	NR	-7.2±14.3	13.5±27.0
Vila et al. [30]	Se (%)	NA	NA	NA	NA	NR	NA	NR	92.6	92.6
	P+ (%)	NA	NA	NA	NA	NR	NA	NR	NR	NR
	LE ($\mu\pm\sigma$) (msec)	NA	NA	NA	NA	NR	NA	NR	-12±23.4	0.8±30.3

Table 5 Performance evaluation of the proposed algorithm on 3-lead 24-hour high resolution Holter data (CHECK #1 and 2)- (LE: Location Error).

Method	Accuracy Parameters	P_{ON}	P_{peak}	P_{OFF}	QRS_{ON}	QRS_{peak}	QRS_{OFF}	T_{ON}	T_{peak}	T_{OFF}
Lead I	(#)	(14310)	(14310)	(14310)	(14310)	(14340)	(14340)	(14310)	(14310)	(14310)
	LE ($\mu\pm\sigma$) (msec) [16]	-4.2±8.3	2.3±11.2	3.1±6.6	-2.4±8.1	3.8±6.7	8.3±11.1	-5.3±9.9	-2.4±7.1	3.8±12.1
	LE ($\mu\pm\sigma$) [13]	-2.7±5.9	1.1±8.3	1.7±4.0	-2.1±5.4	2.1±3.9	5.1±7.7	-2.9±7.1	-1.8±6.6	2.8±4.5
	LE ($\mu\pm\sigma$) [This Study]	-2.3±5.1	1.0±4.1	1.1±2.1	-2.1±4.3	2.1±2.6	5.1±6.8	-2.4±7.0	-1.7±5.3	2.0±3.7
Lead II	(#)	(14293)	(14293)	(14293)	(14307)	(14307)	(14307)	(14293)	(14293)	(14293)
	LE ($\mu\pm\sigma$) (msec) [16]	-4.3±8.8	2.6±11.1	3.0±7.1	-2.6±8.2	3.6±6.1	8.7±11.2	-5.7±9.1	-2.5±7.0	4.9±14.1
	LE ($\mu\pm\sigma$) [13]	-3.4±6.9	1.8±7.1	2.1±3.9	0.9±5.8	1.0±4.5	5.7±9.5	-3.6±4.7	-1.0±4.3	2.8±9.5
	LE ($\mu\pm\sigma$) [This Study]	-2.9±6.1	1.1±5.9	1.8±2.7	0.9±3.9	1.0±3.1	5.7±8.2	-3.1±3.3	-0.7±3.4	2.3±8.4
Lead III	(#)	(14315)	(14315)	(14315)	(14296)	(14296)	(14296)	(14287)	(14287)	(14287)
	LE ($\mu\pm\sigma$) (msec) [16]	-5.6±7.4	4.1±9.6	2.9±5.8	-3.1±7.8	4.7±7.6	7.1±12.0	-5.8±10.8	-1.4±11.1	3.1±10.9
	LE ($\mu\pm\sigma$) [13]	-2.5±4.7	1.8±5.1	0.6±3.2	-1.4±3.3	2.1±5.2	3.4±4.2	-3.4±6.1	-0.6±4.9	0.8±4.8
	LE ($\mu\pm\sigma$) [This Study]	2.2±3.5	1.1±4.0	0.4±2.4	-1.4±2.7	2.1±3.5	3.4±3.1	-2.8±5.0	-0.4±3.4	0.6±4.0

Table 6 Performance characteristics of some proposed detection-delineation algorithms to be compared with each other, (NA: Not Applicable).

Detection Algorithm	Development Environment	Speed Samples/sec	Detection /Delineation	Dependency of Parameters to Sampling Frequency	Maximum Delineation Error msec (RMS)	Se /P+ (%)
Conventional Hilbert Transform [12]	Matlab	52,710	Yes/No	Yes	NA	99.61/99.42
Modified Hilbert Transform [11]	Matlab	43,830	Yes/No	Yes	NA	99.70/99.75
Conventional Discrete Wavelet Transform [15]	Matlab	47,934	Yes/Yes	Yes	12.33	99.80/99.86
DWT-based Area Curve Length Method [16]	C++/MEX (Matlab)	101,701	Yes/Yes	Yes	7.26	99.91/99.88
DWT-based Multiple Higher Order Moments Method [13]	C++/MEX (Matlab)	148,943	Yes/Yes	Yes	6.14	99.94/99.91
MDWM (This Study)	C++/MEX (Matlab)	163,348	Yes/Yes	No	5.29	99.96/99.96

4 Conclusion

The aim of this study was to address a new long-duration holter ECG events detection-delineation algorithm based on the false-alarm error bounded segmentation of a decision statistic. To meet this end, first three-lead holter data was pre-processed by calculation of the Euclidean norm between corresponding samples of three leads. Then, á trous discrete wavelet transform (DWT) was applied to the resulted norm and an unscented synthetic measure was calculated between some obtained dyadic scales. Afterwards, a uniform length window was slid sample to sample on the synthetic scale and in each slid, MDWM of the excerpted segment was calculated. In the next step, a α-level Neyman-Pearson classifier was designed and implemented to detect and delineate QRS complexes. The presented method was applied to MITDB, QTDB, and TWADB and as a result, the average values of sensitivity and positive predictivity Se = 99.96% and P+ = 99.96% were obtained for the detection of QRS complexes, with the average maximum delineation error of 5.7 msec, 3.8 msec and 6.1 msec for P-wave, QRS complex and T-wave, respectively. Also, the proposed method was applied to DAY hospital high resolution holter data and average values of Se=99.98% and P+=99.97% were obtained for QRS detection. In summary, marginal performance improvement of ECG events detection-delineation process in a widespread values of signal to noise ratio (SNR), reliable robustness against strong noise, artifacts and probable severe arrhythmia(s) of high resolution holter data and the processing speed 163,000 samples/sec can be mentioned as important merits and capabilities of the proposed algorithm.

References

[1] Ghaffari A. and Homaeinezhad M. R., "Fading Parameters of Sodium, Potassium and Leakage Ionic Channels the Best Linear Unbiased Sequentially Estimation (BLUE) Via Voltage Clamp Technique Noisy Measurement", *16th. Annual (International) Conference on Mechanical Engineering-ISME,* Shahid Bahonar University of Kerman, Iran, pp. 14-16, May 2008.

[2] Ghaffari A., Homaeinezhad M. R., Atarod M., Ahmady Y. and Rahmani R., "Detecting and Quantifying T-wave Alternans Using the Correlation Method and Comparison with the FFT-based Method", *34th Annual Conference of Computers in Cardiology (CinC),* Bologna, Italy, pp. 14-17, September 2008.

[3] Ghaffari A., Homaeinezhad M. R., Akraminia M., Atarod M. and Daevaeiha M., "Detecting and Quantifying T-Wave Alternans in Patients with Heart Failure and Non-Ischemic Cardiomyopathy via Modified Spectral Method", *35th Annual Conference of Computers in Cardiology (CinC),*

Lake City-Utah, USA, pp. 13-16, September 2009.

[4] Ghaffari A., Homaeinezhad M. R., Akraminia M., Atarod M. and Daevaeiha M., "Detecting and Discriminating Premature Atrial and Ventricular Contractions: Application to Prediction of Paroxysmal Atrial Fibrillation", *35th Annual Conference of Computers in Cardiology (CinC)*, Lake City-Utah, USA, pp. 13-16, September. 2009.

[5] Chiarugi F., Varanini M., Cantini F., Conforti F. and Vrouchos G., "Noninvasive ECG as a Tool for Predicting Termination of Paroxysmal Atrial Fibrillation", *IEEE Transactions on Biomedical Engineering*, Vol. 54, No. 8, pp. 1399-1406, August 2007.

[6] Christov I. and Simova I., "Q-onset and T-end delineation: assessment of the performance of an automated method with the use of a reference database", *Physiological Measurement*, Vol. 28, No. 2, pp. 213-221, 2007.

[7] Minhas F. A. A. and Arif M., "Robust electrocardiogram (ECG) beat classification using discrete wavelet transform", *Physiological Measurement*, Vol. 29, No. 5, pp. 555-570, 2008.

[8] Moniri M. R., Nayebi M. M. and Sheikhi A., "Adaptive Signal Detection in Auto-Regressive Interference with Gaussian Spectrum", *Iranian Journal of Electrical & Electronic Engineering(IJEEE)*, Vol. 4, No. 4, pp. 140-149, 2008.

[9] Sayadi O. and Shamsollahi M. B., "A model-based Bayesian framework for ECG beat Segmentation", *Physiological Measurement*, Vol. 30, No. 3, pp. 335-352, 2009.

[10] Arzeno N. M., Deng Z.-D. and Poon C.-S., "Analysis of First-Derivative Based QRS Detection Algorithms", *IEEE Transactions on Biomedical Engineering*, Vol. 55, No. 2, pp. 478-484, February 2008.

[11] Ghaffari A., Homaeinezhad M. R., Atarod M. and Akraminia M., "Parallel Processing of ECG and Blood Pressure Waveforms for Detection of Acute Hypotensive Episodes: A Simulation Study Using a Risk Scoring Model", *Computer Methods in Biomechanics and Biomedical Engineeing*, Taylor & Francis Publishing, In-Press, 2009.

[12] Benitez D., Gaydeckia P. A., Zaidib A. and Fitzpatrickb A. P., "The use of the Hilbert transform in ECG signal analysis", *Computers in Biology and Medicine*, Vol. 31, No. 5, pp. 399-406, 2001.

[13] Ghaffari A., Homaeinezhad M. R., Khazraee M. and Daevaeiha M., "Segmentation of Holter ECG Waves via Analysis of a Discrete Wavelet-Derived Multiple Skewness-Kurtosis Based Metric", *Annals of Biomedical Engineering*, Springer Publishing, In-Press, 2010.

[14] Mitra M. and Mitra S., "A Software Based Approach for Detection of QRS Vector of ECG Signal", *IFMBE Proceedings*, Vol. 15, pp. 348-351, 2007.

[15] Martinez J. P., Almeida R., Olmos S., Rocha A. P. and Laguna P., "A Wavelet-Based ECG Delineator: Evaluation on Standard Databases", *IEEE Transactions on Biomedical Engineering*, Vol. 51, No. 4, pp. 570-581, 2004.

[16] Ghaffari A., Homaeinezhad M. R., Akraminia M., Atarod M. and Daevaeiha M., "A Robust Wavelet-based Multi-Lead Electrocardiogram Delineation Algorithm", *Medical Engineering & Physics*, Vol. 31, No. 10, pp. 1219-1227, 2009.

[17] Ghaffari A., Homaeinezhad M. R., Akraminia M. and Daevaeiha M., "Finding Events of Electrocardiogram and Arterial Blood Pressure Signals Via Discrete Wavelet Transform with Modified Scales", *Imeche Proceedings, Part H: Engineering in Medicine*, In-Press, 2009.

[18] Kannathal N., Lim C. M., Acharya U. R. and Sadasivan P. K., "Cardiac state diagnosis using adaptive neuro fuzzy technique", *Medical Engineering & Physics*, Vol. 28, No. 8, pp. 809-815, 2006.

[19] de Lannoy G., Frenay B., Verleysen M., Delbeke J., "Supervised ECG Delineation Using the Wavelet Transform and Hidden Markov Models", *The Proceedings of IFMBE*, Vol. 22, pp. 22-25, 2008.

[20] Moody G. B. and Mark R. G., "The MIT-BIH Arrhythmia Databaseon CD-Rom and Software for it", *The Proseeding of Computers in Cardiology*, pp. 185-188, 1990.

[21] Laguna P., Mark R., Goldenberger A. and Moody G. B., "A Database for Evaluation of Algorithms for Measurement of QT and Other Waveform intervals in ECG", *The Proceeding of Computers in Cardiology*, pp. 673-676, 1997.

[22] Taddei A., Distante G., Emdin M., Pisani P., Moody G. B., Zeelenberg C. and Marchesi C., "The European ST-T Database: Standards for Evaluating Systems for the Analysis of ST-T Changes in Ambulatory Electrocardiography", *European Heart Journal*, Vol. 13, No. 9, pp. 1164-1172, 1992.

[23] Moody G. B., "The PhysioNet/Computers in Cardiology Challenge 2008: T-Wave Alternans", *The Proceeding of Computers in Cardiology*, Vol. 35, pp. 505-508, 2008.

[24] Moody G. B., *WFDB Applications Guide*, Tenth Edition, Harvard-MIT Division of Health Sciences and Technology, 2006. (*http://www.physionet.org/physiotools/wag/*)

[25] Li C., Zheng C. and Tai C., "Detection of ECG Characteristic Points using Wavelet Transforms", *IEEE Transactions on Biomedical Engineering*, Vol. 42, No. 1, pp. 21-28, 1995.

[26] Hamilton P. S. and Tompkins W., "Quantitative Investigation of QRS Detection Rules using the MIT/BIH Arrhythmia Database", *IEEE Transactions on Biomedical Engineering*, Vol. 33, No. 12, pp. 1157-1165, 1986.

[27] Pan J. and Tompkins W. J., "A Real-Time QRS Detection Algorithm", *IEEE Transactions on Biomedical Engineering*, Vol. 32, pp. 230-236, 1985.

[28] Moody G. B. and Mark R. G., "Development and Evaluation of a 2-Lead ECG Analysis Program", *The Proceeding of Computers in Cardiology*, pp. 39-44, 1982.

[29] Laguna P., Jane R. and Caminal P., "Automatic Detection of Wave Boundaries in Multi Lead ECG Signals: Validation with the CSE Database", *Computers and Biomedical Research*, Vol. 27, No. 1, pp. 45-60, 1994.

[30] Vila J., Gang Y., Presedo J., Fernandez-Delgado M. and Malik M., "A New Approach for TU Complex Characterization", *IEEE Transactions on Biomedical Engineering*, Vol. 47, No. 6, pp. 764-772, 2000.

[31] Montgomery D. C. and Runger G. C., *Applied Statistics and Probability for Engineers*, Third Edition, John Wiley & Sons, 2003.

[32] Bishop C. M., *Pattern Recognition and Machine Learning*, Springer Publishing, 2006.

[33] Kay S. M., *Fundamentals of Statistical Signal Processing: Estimation Theory*, Prentice- Hall Inc. 1979.

[34] Vincent Poor H., *An Introduction to Signal Detection and Estimation*, Second Edition, Chapters 1-3, Springer-Verlag, 1994.

[35] *http://www.physionet.org/physiobank/database/*.

Mohammad Reza Homaeinezhad was born in Shiraz, Iran, in 1980. He received his BSc, MSc and Ph.D. degrees (with the best honors) all in Mechanical Engineering, Dynamic systems and control, in 2003, 2005, 2010, respectively from K. N. Toosi University of Technology, Tehran, Iran. Since September 2010, he has been an assistant professor of Mechanical Engineering (bio-mechatronics) at K. N. Toosi University of Technology and his research interests include nonlinear dynamics and control, statistical signal analysis and parameter estimation, automatic decision making (detection & modulation) theory and biomedical waveforms (BP, ECG & PCG) processing.
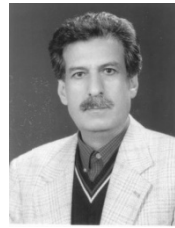
Ali Ghaffari was born in Neyshabour in 1945. He received the BSc, MSc and Ph.D. all in Mechanical Engineering from Sharif University of Technology, Georgia Institute of Technology and University of California at Berkeley in 1969, 1973 and 1976, respectively. Since, 1979 he has been with the department of Mechanical Engineering of K. N. Toosi University of Technology. Professor Ghaffari's research is mainly focused on dynamic systems and control including analysis of stochastic phenomena, dynamics and control of nonlinear systems, application of fuzzy set theory and artificial neural networks to mechanical systems, and biomedical signal processing, specifically ECG.

Hamid Najjaran Toosi was born in Mashhad, Iran in 1981. He received the BSc and the MSc degrees in Computer-software engineering and Machatronic engineering from Mashhad Islamic Azad university and K. N. Toosi University of Technology, respectively in 2005 and 2008. Since 2008 he has been a member of the CardioVascular Research Group (CVRG) as a computer programmer for software engineering and structured databases. His research interest include artificial intelligence and pattern recognition, data structure, high-speed programming.

Maryam Tahmasebi. Medical doctor of cardiology. At publication time, no photograph and biography were available.

Mohammad Mehdi Daevaeiha was born in Esfahan, Iran, in 1981. He received his BSc, MSc degrees in Mechanical Engineering, Dynamic system and control in 2004 and 2007 respectively. He is currently assistant director of Non-Invasive Cardiac Electrophysiology Research Lab. at the Day General Hospital, Tehran-Iran and his research interests including non-invasive cardiac electrophysiology (Sudden Cardiac Death (SCD) risk stratification), Enhanced External Counter Pulsation (EECP) (acute effect and development of improved therapy), mechanical characteristic of heart (Cardiac Elastance), biomedical signal processing (detection and de-noising).